



Hydrodynamic instability growth and mix experiments at the National Ignition Facility

V. A. Smalyuk, M. Barrios, J. A. Caggiano, D. T. Casey, C. J. Cerjan, D. S. Clark, M. J. Edwards, J. A. Frenje, M. Gatu-Johnson, V. Y. Glebov, G. Grim, S. W. Haan, B. A. Hammel, A. Hamza, W. W. Hsing, O. Hurrucane, J. D. Kilkenny, J. L. Kline, J. P. Knauer, O. L. Landen, J. D. Lindl, T. Ma, J. M. McNaney, M. Mintz, A. Moore, A. Nikroo, T. Parham, J. L. Peterson, R. Petrasso, L. Pickworth, J. E. Pino, K. Raman, S. P. Regan, B. A. Remington, H. F. Robey, D. P. Rowley, D. B. Sayre, R. E. Tipton, S. V. Weber, K. Widmann, D. C. Wilson, C. B. Yeamans

December 3, 2013

Physics of Plasmas

Disclaimer

This document was prepared as an account of work sponsored by an agency of the United States government. Neither the United States government nor Lawrence Livermore National Security, LLC, nor any of their employees makes any warranty, expressed or implied, or assumes any legal liability or responsibility for the accuracy, completeness, or usefulness of any information, apparatus, product, or process disclosed, or represents that its use would not infringe privately owned rights. Reference herein to any specific commercial product, process, or service by trade name, trademark, manufacturer, or otherwise does not necessarily constitute or imply its endorsement, recommendation, or favoring by the United States government or Lawrence Livermore National Security, LLC. The views and opinions of authors expressed herein do not necessarily state or reflect those of the United States government or Lawrence Livermore National Security, LLC, and shall not be used for advertising or product endorsement purposes.

**Hydrodynamic instability growth and mix experiments at the National Ignition
Facility**

V. A. Smalyuk¹, M. Barrios¹, J. A. Caggiano¹, D. T. Casey¹, C. J. Cerjan¹, D. S. Clark¹,
M. J. Edwards¹, J. A. Frenje², M. Gatu-Johnson², V. Y. Glebov³, G. Grim⁴, S. W. Haan¹,
B. A. Hammel¹, A. Hamza¹, W. W. Hsing¹, O. Hurricane¹, J. D. Kilkenny⁵, J. L. Kline⁴,
J. P. Knauer³, O. L. Landen¹, J. D. Lindl¹, T. Ma¹, J. M. McNaney¹, M. Mintz¹, A.
Moore⁶, A. Nikroo⁵, T. Parham¹, J. L. Peterson¹, R. Petrasso², L. Pickworth¹, J. E. Pino¹,
K. Raman¹, S. P. Regan³, B. A. Remington¹, H. F. Robey¹, D. P. Rowley¹, D. B. Sayre¹,
R. E. Tipton¹, S. V. Weber¹, K. Widmann¹, D. C. Wilson⁴, and C. B. Yeamans¹

¹Lawrence Livermore National Laboratory, NIF Directorate, Livermore, CA 94550, USA

²Massachusetts Institute of Technology, Cambridge, MA 02139, USA

³Laboratory for Laser Energetics, University of Rochester, Rochester, NY 14623, USA

⁴Los Alamos National Laboratory, Los Alamos, NM 97544, USA

⁵General Atomics, San Diego, CA 92186, USA

⁶AWE Aldermaston, Reading, Berkshire, RG7 4PR, United Kingdom.

ABSTRACT

Hydrodynamic instability growth and its effects on implosion performance were studied at the National Ignition Facility (NIF) [G. H. Miller, E. I. Moses and C. R. Wuest, *Opt. Eng.* **443**, 2841 (2004)]. Implosion performance and mix have been measured at

peak compression using plastic shells filled with tritium gas and imbedding localized CD diagnostic layer in various locations in the ablator. Neutron yield and ion temperature of the DT fusion reactions were used as a measure of shell-gas mix, while neutron yield of the TT fusion reaction was used as a measure of implosion performance. The results have indicated that the low-mode hydrodynamic instabilities due to surface roughness were the primary culprits to yield degradation, with atomic ablator-gas mix playing a secondary role. In addition, spherical shells with pre-imposed 2D modulations were used to measure instability growth in the acceleration phase of implosions. The capsules were imploded using ignition-relevant laser pulses, and ablation-front modulation growth was measured using x-ray radiography for a shell convergence ratio of ~ 2 . The measured growth was in good agreement with that predicted, thus validating simulations for the fastest growing modulations with mode numbers up to 90 in the acceleration phase. Future experiments will be focused on measurements at higher convergence, higher-mode number modulations, and during the deceleration phase.

I. INTRODUCTION

The goal of inertial confinement fusion (ICF) [1-3] is to implode a spherical target to achieve high compression of the deuterium-tritium (DT) fuel and high temperature in the hot spot, to trigger ignition and produce significant thermonuclear energy gain. Hydrodynamic instabilities and mix play a central role in the performance degradation of the spherical implosions in inertial confinement fusion (ICF) [2,3]. In indirect-drive ICF implosion experiments at the National Ignition Facility (NIF) [4], the laser drive was converted into x rays inside a high-Z enclosure (hohlraum) to drive the spherical plastic

capsules containing layered DT fuel layers [2,3]. The implosion begins with an acceleration phase when the x-rays ablate the shell surface and the capsule accelerates and starts to converge. Outer-shell nonuniformities grow as a result of the acceleration-phase Richtmyer-Meshkov (RM) [5,6] and Rayleigh–Taylor (RT) instabilities [7,8] at this stage of implosion [9-26]. As the shell accelerates, these front-surface perturbations feed through the shell, seeding perturbations on an ablator-ice interface and an inner-ice surface [2,3]. At this time, ablator jets from localized surface perturbations can penetrate the shell and mix ablator material into the DT hot spot [27]. As the shell approaches its center, it starts to decelerate due to inner gas pressure while continuing to converge. At stagnation, the shell stops (at peak compression) and then rebounds. During the deceleration phase, the inner surface of the shell and the ablator-ice interface are subjects to hydrodynamic instabilities [28-35]. At this phase, the drive asymmetries and surface imperfections are further amplified by the instabilities resulting in a distorted shell with reduced hot-spot temperature, volume, and pressure [36]. The modulations also grow due to Bell–Plesset (BP) convergent effects throughout the compression [37].

In recent high-compression experiments on NIF, high fuel areal densities (up to $\sim 1.3 \text{ g/cm}^2$) have been achieved with fuel velocities of $\sim 320\text{-}330 \text{ km/s}$ [36,38]. These key performance parameters were close to the goal of the ignition design, while the neutron yields were reduced by hydrodynamic instabilities and drive asymmetries [36,38]. The presence of mixed ablator material was also correlated with reduced experimental yields and temperatures in high-compression layered DT implosions [39,40]. Multidimensional (2D and 3D) simulations of the layered deuterium-tritium (DT) implosions intended to capture performance degradation due to instabilities and drive asymmetries. They over-

predicted measured yields by factors up to ~ 30 for high-compression implosions [41]. However, 2D simulations with large, un-physical multipliers (up to 3-5x) on the capsule surface roughness could bring simulated yields down to the measured levels [42]. These results demonstrated a need to quantitatively understand the instability growth in experiments and simulations before a strategy to mitigate them can be designed in high-compression implosions.

Several experimental platforms are being developed to measure and understand various aspects of the instability growth and mix in the ignition-relevant conditions on NIF. They include experiments to measure instabilities in both acceleration and deceleration phases of implosions, at outer-ablator and ablator-ice interfaces using various experimental techniques including x-ray imaging, x-ray spectroscopy, and nuclear techniques. This article reviews experimental results from two campaigns that measured instability growth at outer ablation surface in the acceleration phase [42] and at shell-gas interface in the deceleration phase of plastic-shell implosions [43]. The ablation-front instability experiments are described in Sec. II; while the atomic-mix experiments near peak compression of the plastic-shell implosions are discussed in Sec. III. The discussion of the results is presented in Sec. IV and summarised in Sec. V.

II. ABLATION-FRONT INSTABILITY EXPERIMENTS

Rayleigh-Taylor growth experiments were designed to measure instability at the acceleration phase of spherical implosions [42] at National Ignition Facility [4]. Figure 1 shows experimental configuration including Au hohlraum, plastic (CH) capsule, Au cone, and the vanadium backlighter. The gold cone provided a possibility for the

backlighter x-rays to pass through a single wall of the shell, enabling high-quality radiographs of the growing modulations. The experimental configuration was similar to previous backlighting experiments on NIF [44]. The differences included the additional gold cone, the backlighter material (vanadium vs. germanium), and the reduced thickness (80- μm vs. 160- μm) of the high-density carbon (HDC) window placed at the hohlraum wall. Figure 2 shows an image of the capsule and the gold cone used in these experiments. The capsules had pre-imposed, 2D sinusoidal modulations at three wavelengths, 240 μm (mode 30), 120 μm (mode 60), and 80 μm (mode 90). The initial modulation amplitudes were in the range from 0.25 μm to 1.7 μm . The experiments were driven with the shaped, 21-ns long laser pulse with peak power of ~ 350 TW and total laser energy of 1.3 MJ (shown in Fig. 3) using 184 beams of the NIF laser system. An additional eight overlapped beams were used to drive a 12.5- μm thick vanadium backlighter foil at peak laser intensity of $\sim 5 \times 10^{14}$ W/cm². The experiments were conducted with the drives and conditions similar to those used in high-compression layered DT implosions [38]. They were designed to test the hydrodynamic growth predictions used to model these DT layered implosions that achieved fuel areal densities of ~ 1.3 g/cm², peak fuel velocities of ~ 320 - 330 km/s, and driven at peak radiation temperatures of ~ 300 eV [38]. The nominal 209- μm thick plastic capsules with nominal 1120- μm outer radii had the same Si-doped layers, as used in the previous DT layered implosion, as previously published in Ref. [38]. An extra 20- μm thick CH layer was used to replace the 69- μm thick DT layer to maintain the same shell mass as in the layered DT implosions. Current experiments followed a campaign that characterized the implosion shock timing and symmetry [35,45,46].

The modulation growth was measured with through-foil x-ray radiography [26] using ~ 5.4 -keV x-rays generated by the vanadium backlighter located 12 mm from the target center [42]. Figure 4 shows capsule x-ray radiographs captured on a framing camera. The central four images of growing capsule modulations were formed using 20- μm wide slit, while images on right and left sides of the slit images were formed with 20- μm and 50- μm pinholes. This experiment was performed with side-by-side mode 60 and mode 90 modulations. The temporal resolution of the framing camera was 100 ps, while spatial resolution of the slit images was 20 μm . The slit and pinholes were positioned 100 mm from the target center, while the detector, a framing camera [47], was located 1300 mm from the target center, giving a magnification of ~ 12 for the imaging system. Pinhole images on the right-hand-side of the Fig. 4 included an attenuation of the 30- μm aluminum strip, used to measure sensitivity of the system. X-ray filters were used in these experiments included 150 μm polyimide and 12.5 μm thick vanadium filters. The measurements were conducted for convergence ratios up to ~ 2 , when the shell radius was decreased down to ~ 550 μm in the implosions. Optical-depth (OD) variations (used in the analysis below) were obtained by taking a natural logarithm of the framing-camera images after x-ray backgrounds were subtracted.

Figure 5 shows measured optical-depth modulation growth for the modes 30 [Fig. 5(a)], 60 [Fig. 5(a)], and 90 [Fig. 5(a)] as a function of the modulation wavelength. As the capsule implodes, the wavelengths of the modulations decrease while the modulation amplitudes increase, so the time increases from the right to left in Figs. 5. The results are compared with simulation predictions post-processed using 5.4-keV backlighter energy, 100-ps temporal resolution, and 20- μm spatial resolution. The measured growth was in

good agreement with that predicted for all three modes. Figure 6 shows measured and calculated modulation optical-depth (OD) growth factors as a function of the modulation mode number at shell radius of 650 μm , corresponding to a measurement time of 20.3 ns. The OD growth factor was defined as ratio of the modulation OD amplitude at the time of the measurement to the initial modulation OD amplitude. Effects of the spatial resolution were taken out in the measured experimental points for fair comparison. The good agreement between simulations and experiments indicated that instability growth was modeled well for the most unstable modulations in the high-convergence layered DT implosions in the acceleration phase at convergence ratios up to ~ 2 .

III. DECELERATION-PHASE MIX EXPERIMENTS

Figure 7 schematically shows two types of capsules used in the atomic-mix spherical implosion experiments [43]. Plastic shells had nominal 209- μm thicknesses and 2280- μm -initial outer diameters. Si-doped layers were used to reduce preheat of the inner CH ablator from M-band emission from the Au hohlraum wall. In the first type of capsules, plastic shells included a CD layers with 4.0- μm thicknesses, placed at either the inner shell surface, or offset by up to 8.0 μm from the inner surface by the CH-only layers, as shown in Fig. 7(a). The capsules were filled with high-purity tritium gas (including a small contamination of deuterium gas of 0.1% by atom fraction) to allow shell-gas atomic mix to be studied using the DT fusion reaction ($\text{D} + \text{T} \rightarrow {}^4\text{He} + \text{n}$) by measuring the DT neutron yield and ion temperature. The background DT yields from this D contamination were measured in additional control implosions that did not contain

the CD layers (“CH capsules”), as shown in Fig. 7(b). The DT reactions from these control implosions were also used as a diagnostic of the central core ion temperature.

All implosions used a laser pulse with peak power of ~ 435 TW and total laser energy of ~ 1.5 MJ (shown in Fig. 8); the same pulse was used in a number of cryogenic layered DT implosions [46]. Details of the laser pulse shape, pointing, and hohlraum geometry were determined in previous experiments as described in Ref. [46]. The capsule and drive parameters were kept very similar in this set of experiments. Capsule thickness and outer diameter varied less than 0.5% and 1.5%, respectively. The laser power profiles were identical to a $\sim 5\%$ level. The performance of all implosions was characterized with a comprehensive set of nuclear and x-ray diagnostics [43]. The x-ray fluxes of hohlraum radiation from the laser entrance hole were measured with the Dante diagnostic [46]; the inferred x-ray flux temperatures were very repeatable, $T_r = 294 \pm 4$ eV in all shots. Measured implosion x-ray bang times were $\sim 22.55 \pm 0.10$ ns, all within 100 ps from each other, with the burn width ~ 300 ps in all shots.

Figure 9 shows an example of the measured neutron spectrum in one of the implosions with CD layer [43,48]. The peak at 14.1 MeV was used to measure both the total DT neutron yield and the ion temperature in the DT producing region, while neutrons below 9 MeV were used to measure TT yield in the central hot spot. Target compression was inferred using the down-scattered ratio (DSR $\sim 1.2\%$) of scattered neutrons in the range from 10 to 12 MeV, relative to primary neutrons in the range from 13 to 15 MeV [43]. Figure 10 shows the measured neutron results and comparisons with ARES simulations [49]. The DT yields, DT ion temperatures, and TT yields are shown in Figs. 10 (a), (b), and (c), respectively. In implosions without CD layers (labeled “CH

capsules”), the measured TT and DT yields along with DT ion temperatures probed the same conditions in the central part of the core. In implosions with CD layers the DT yields were up to ~6 times higher, and DT ion temperatures were lower (~ 2.0 keV vs 3.4 keV), compared to “CH capsules.” The lower measured temperature supports the hypothesis that the DT neutrons were primarily generated in the colder region near the shell-gas interface where D and T were atomically mixed. As the recession of the CD layers from the inner surface increased, the measured DT yields decreased, indicating that much of the plastic mixed into the gas came from a region close to the inner surface. The TT yields were similar in all implosions with and without CD layers, indicating excellent experimental repeatability.

The experimental results were compared with 2D simulations using the code ARES [49]. To capture large wavelength, low-mode ($l \llsim 100$) instabilities, direct numerical simulations were performed with imposed surface roughness at unstable interfaces. The K-L mix model [50] (where K represents turbulent kinetic energy, and L is the spatial scale of the mixing layer) was included to capture the turbulent regime and the effects of mix at scales smaller than the computational grid. The free parameter in this method was the initial turbulent mixing length, L_0 , set at all unstable interfaces. As shown in Fig.10, the simulations match well the whole set of experiments. For this, a multiplier of 3 times on the nominal outer surface roughness was needed to match the measured conditions in the central hot core, as determined by the TT yield. The measured outer surface roughness in these experiments varied from 0.5 to almost 2 times the nominal value used in our simulations; thus the 3x nominal values needed to match the TT yield represent up to a factor of ~6 above the measured roughness. This need for a

multiplier is consistent with previous 2D simulations of high-compression layered DT implosions [3]. To explain the conditions in outer colder core (DT yield and ion temperature), a low roughness parameter of $L_0=0.1$ nm was used in the K-L mix model. These results indicated that the low-mode hydrodynamic instabilities due to surface non-uniformities were the primary reason to yield degradation, with atomic ablator-gas mix playing a secondary role.

IV. DISCUSSION

In recent high-compression experiments on NIF, a fuel areal density of ~ 1.3 g/cm² has been achieved with a fuel velocity of ~ 320 - 330 km/s [42]. While these two key performance parameters were close to the ignition goals, the neutron yield was significantly lower than predicted [42]. Original multidimensional simulations of the layered deuterium-tritium (DT), high-compression implosions intending to capture performance degradation due to instabilities and drive asymmetries over-predicted measured yields by factors of ~ 5 to ~ 30 [50]. Two-dimensional simulations with large, multipliers (up to $\sim 5x$) on the capsule surface roughness could bring simulated yields down to the measured levels [50]. This prompted the hypothesis that the instability growth factors were larger than in simulations.

As shown in Sec. III, the implosion experiments using plastic capsules with CD layers and filled tritium gas measured performance of lower-convergence (compared to layered DT) implosions and directly measured ablator atomic mix using the DT nuclear reaction. Two-dimensional simulations of these experiments [43], which included the turbulent K-L mix model [50] to capture the effects of high-mode mix, could explain the

experimental results, but still required large surface roughness multipliers, consistent with modeling of high-compression layered DT implosions. These atomic-mix experiments suggested that low-mode (with Legendre mode numbers $l < 100$) hydrodynamic instabilities were the primary cause of yield degradation, with atomic ablator-gas mix playing a secondary role.

There were several possible explanations for the need for large multipliers on the initial surface perturbation. The effective roughness could have been larger than assumed based on current metrology methods. The Rayleigh-Taylor [7,8] growth rates during the acceleration phase, or the pre-acceleration amplitudes established during the Richtmyer-Meshkov [5,6] instability phase could also be larger than simulated. Some possible seeds for instability growth, such as radiation asymmetry [1], dust grains and other localized defects, and the effect of the membrane (“tent”) used to support the capsule [52,53] were not included or were underestimated in the simulations. The resultant elevated modulations could cause stronger performance degradation at peak compression, as suggested in recent simulations [54,55]. In order to explain past results and inform future designs, predictions of hydrodynamic instability growth needed to be tested and validated by experiments.

As shown in Sec. II, the first experiments to directly measure ablation-front hydrodynamic growth using x-ray radiography of pre-imposed, 2D sinusoidal perturbations were performed at NIF. The goal was to test hydrodynamic growth in simulations during both the Richtmyer-Meshkov phase and the Rayleigh-Taylor phase at the outer ablation surface with moderate capsule convergence (2-3). The measured

growth was in good agreement with that predicted, thus validating simulations for the fastest growing modulations with mode numbers up to 90 in the acceleration phase.

Recent, fully integrated, 2D and 3D simulations generally were unable to fully include the effects of ablator jets in the DT fuel [50,55], but the presence of mixed ablator material was correlated with reduced experimental yields and temperatures in the high-compression layered DT implosions [39,40]. This supported another hypothesis that ablator jet mix [27] was also a major contributor to yield degradation. Future radiography experimenters are planned to address this physics by measuring growth factors of high-mode modulations, representative of the modulations that can produce ablator jets into the DT hot spot. In addition, the ablation-front radiography measurements will be extended to the time of peak shell velocity, testing code predictions of the ablation-surface growth simulation up to the end of acceleration phase at convergence ratios up to ~ 5 . They will be conducted with 3D modulations representative of the surface roughness and imperfections in the recent layered DT implosions. Additional experiments are also planned to measure modulation growth and jet-related mix in the deceleration phase with pre-imposed 2D, 3D modulations, and with spectroscopic layers, extending previous time-integrated mix measurements [39,40] including a capability of temporal resolution of the mix and also better spatial resolution.

V. CONCLUSIONS

Hydrodynamic instability growth and its effects on implosion performance and mix were studied at the National Ignition Facility. The results of atomic-mix experiments using plastic shells with CD layers have indicated that the low-mode hydrodynamic

instabilities due to surface roughness were the primary culprits to yield degradation in plastic shell implosions, with atomic ablator-gas mix playing a secondary role. Hydrodynamic instability growth measurements with pre-imposed modulations were performed to test predictions of the Rayleigh-Taylor unstable growth in implosions with convergence ratio of ~ 2 . The measured growth was in good agreement with that predicted, thus validating simulations for the fastest growing modulations with mode numbers up to 90 in the acceleration phase. Future acceleration-phase instability experiments will be extended to shorter wavelengths and to higher convergence ratios up to ~ 5 . In addition, deceleration phase instability experiments are also planned to test and validate simulation predictions near peak compression of the spherical implosions.

ACKNOWLEDGMENT

This work was performed under the auspices of the U.S. Department of Energy by Lawrence Livermore National Laboratory under Contract DE-AC52-07NA27344.

REFERENCES

- [1] J. Nuckolls, L. Wood, A. Thiessen, and G. Zimmerman, *Nature* **239**, 139 (1972).
- [2] S. Atzeni and J. Meyer-ter-Vehn, *The Physics of Inertial Fusion: Beam Plasma Interaction, Hydrodynamics, Hot Dense Matter*, International Series of Monographs on Physics (Clarendon Press, Oxford, 2004).
- [3] J. D. Lindl, *Inertial Confinement Fusion: The Quest for Ignition and Energy Gain Using Indirect Drive* (Springer-Verlag, New York, 1998).

- [4] E. I. Moses, R. N. Boyd, B. A. Remington, C. J. Keane, and R. Al-Ayat, *Phys. Plasmas* **16**, 041006 (2009); G. H. Miller, E. I. Moses and C. R. Wuest, *Opt. Eng.* **43**, 2841 (2004).
- [5] R. D. Richtmyer, *Commun. Pure Appl. Math.* **13**, 297 (1960).
- [6] E. E. Meshkov, *Izv. Acad. Sci. USSR Fluid Dynamics* **4**, 101 (1969).
- [7] Lord Rayleigh, *Proc. London Math Soc.* **XIV**, 170 (1883).
- [8] G. Taylor, *Proc. R. Soc. London Ser. A* **201**, 192 (1950).
- [9] S. G. Glendinning, S. N. Dixit, B. A. Hammel, D. H. Kalantar, M. H. Key, J. D. Kilkenny, J. P. Knauer, D. M. Pennington, B. A. Remington, R. J. Wallace, and S. V. Weber, *Phys. Rev. Lett.* **78**, 3318 (1997).
- [10] K. S. Budil, B. A. Remington, T. A. Peyser, K. O. Mikaelian, P. L. Miller, N. C. Woolsey, W. M. Wood-Vasey, and A. M. Rubenchik, *Phys. Rev. Lett.* **76**, 4536 (1996).
- [11] K. S. Budil, B. Lasinski, M. J. Edwards, A. S. Wan, B. A. Remington, S. V. Weber, S. G. Glendinning, L. Suter, and P. E. Stry, *Phys. Plasmas* **8**, 2344 (2001).
- [12] B. A. Remington, S. V. Weber, M. M. Marinak, S. W. Haan, J. D. Kilkenny, R. Wallace, and G. Dimonte, *Phys. Rev. Lett.* **73**, 545 (1994).
- [13] M. M. Marinak, S. G. Glendinning, R. J. Wallace, B. A. Remington, K. S. Budil, S. W. Haan, R. E. Tipton, and J. D. Kilkenny, *Phys. Rev. Lett.* **80**, 4426 (1998).
- [14] J. Grun, M. E. Emery, C. K. Manka, T. N. Lee, E. A. McLean, A. Mostovych, J. Stamper, S. Bodner, S. P. Obenschain, and B. H. Ripin, *Phys. Rev. Lett.* **58**, 2672 (1987).

- [15] K. Shigemori, H. Azechi, M. Nakai, M. Honda, K. Meguro, N. Miyanaga, H. Takabe, and K. Mimi, *Phys. Rev. Lett.* **78**, 250 (1997).
- [16] J. P. Knauer, R. Betti, D. K. Bradley, T. R. Boehly, T. J. B. Collins, V. N. Goncharov, P. W. McKenty, D. D. Meyerhofer, V. A. Smalyuk, C. P. Verdon, S. G. Glendinning, D. H. Kalantar, and R. G. Watt, *Phys. Plasmas* **7**, 338 (2000).
- [17] R. J. Taylor, J. P. Dahlburg, A. Iwase, J. H. Gardner, D. E. Fyfe, and O. Willi, *Phys. Rev. Lett.* **76**, 1643 (1996).
- [18] D. H. Kalantar, M. H. Key, L. B. Da Silva, S. G. Glendinning, B. A. Remington, J. E. Rothenberg, F. Weber, S. V. Weber, E. Wolfrum, N. S. Kim, D. Neely, J. Zhang, J. S. Wark, A. Demir, J. Lin, R. Smith, G. J. Tallents, C. L. S. Lewis, A. MacPhee, J. Warwick, and J. P. Knauer, *Phys. Plasmas* **4**, 1985 (1997).
- [19] H. Azechi, M. Nakai, K. Shigemori, N. Miyanaga, H. Shiraga, H. Nishimura, M. Honda, R. Ishizaki, J. G. Wouchuk, H. Takabe, K. Nishihara, K. Mima, A. Nishiguchi, and T. Endo, *Phys. Plasmas* **4**, 4079 (1997).
- [20] C. J. Pawley, S. E. Bodner, J. P. Dahlburg, S. P. Obenschain, A. J. Schmitt, J. D. Sethian, C. A. Sullivan, J. H. Gardner, Y. Aglitskiy, Y. Chan, and T. Lehecka, *Phys. Plasmas* **6**, 565 (1999).
- [21] V. A. Smalyuk, T. R. Boehly, D. K. Bradley, V. N. Goncharov, J. A. Delettrez, J. P. Knauer, D. D. Meyerhofer, D. Oron, and D. Shvarts, *Phys. Rev. Lett.* **81**, 5342 (1998).
- [22] T. R. Boehly, V. N. Goncharov, O. Gotchev, J. P. Knauer, D. D. Meyerhofer, D. Oron, S. P. Regan, Y. Srebro, W. Seka, D. Shvarts, S. Skupsky, and V. A. Smalyuk, *Phys. Plasmas* **8**, 2331 (2001).

- [23] V. A. Smalyuk, O. Sadot, J. A. Delettrez, D. D. Meyerhofer, S. P. Regan, and T. C. Sangster, *Phys. Rev. Lett.* **95**, 215001 (2005).
- [24] V. A. Smalyuk, O. Sadot, R. Betti, V. N. Goncharov, J. A. Delettrez, D. D. Meyerhofer, S. P. Regan, T. C. Sangster, and D. Shvarts, *Phys. Plasmas* **13**, 056312 (2006).
- [25] O. Sadot, V. A. Smalyuk, J. A. Delettrez, D. D. Meyerhofer, T. C. Sangster, R. Betti, V. N. Goncharov, and D. Shvarts, *Phys. Rev. Lett.* **95**, 265001 (2005).
- [26] V. A. Smalyuk, S. X. Hu, J. Hager, J. A. Delettrez, D. D. Meyerhofer, T. C. Sangster, and D. Shvarts, *Phys. Rev. Lett.* **103**, 105001 (2009).
- [27] B. A. Hammel, H. A. Scott, S. P. Regan, C. Cerjan, D. S. Clark, M. J. Edwards, R. Epstein, S. H. Glenzer, S. W. Haan, N. Izumi, J. A. Koch, G. A. Kyrala, O. L. Landen, S. H. Langer, K. Peterson, V. A. Smalyuk, L. J. Suter, and D. C. Wilson, *Phys. Plasmas* **18**, 056310 (2011).
- [28] H. Sakagami and K. Nishihara, *Phys. Rev. Lett.* **65**, 432 (1990).
- [29] R. P. J. Town and A. R. Bell, *Phys. Rev. Lett.* **67**, 1863 (1991).
- [30] M. M. Marinak, R. E. Tipton, O. L. Landen, T. J. Murphy, P. Amendt, S. W. Haan, S. P. Hatchett, C. J. Keane, R. McEachern, and R. Wallace, *Phys. Plasmas* **3**, 2070 (1996).
- [31] V. Lobatchev and R. Betti, *Phys. Rev. Lett.* **85**, 4522 (2000).
- [32] M. C. Herrmann, M. Tabak, and J. D. Lindl, *Phys. Plasmas* **8**, 2296 (2001).
- [33] V. A. Smalyuk, V. N. Goncharov, J. A. Delettrez, F. J. Marshall, D. D. Meyerhofer, S. P. Regan, and B. Yaakobi, *Phys. Rev. Lett.* **87**, 155002 (2001).

- [34] R. Betti, K. Anderson, V. N. Goncharov, R. L. McCrory, D. D. Meyerhofer, S. Skupsky, and R. P. J. Town, *Phys. Plasmas* **9**, 2277 (2002).
- [35] V. A. Smalyuk, J. A. Delettrez, V. N. Goncharov, F. J. Marshall, D. D. Meyerhofer, S. P. Regan, T. C. Sangster, R. P. J. Town, and B. Yaakobi, *Phys. Plasmas* **9**, 2738 (2002).
- [36] M. J. Edwards, P. K. Patel, J. D. Lindl, L. J. Atherton, S. H. Glenzer, S. W. Haan, J. D. Kilkenny, O. L. Landen, E. I. Moses, A. Nikroo, R. Petrasso, T. C. Sangster, P. T. Springer, S. Batha, R. Benedetti, L. Bernstein, R. Betti, D. L. Bleuel, T. R. Boehly, D. K. Bradley, J. A. Caggiano, D. A. Callahan, P. M. Celliers, C. J. Cerjan, K. C. Chen, D. S. Clark, G. W. Collins, E. L. Dewald, L. Divol, S. Dixit, T. Doeppner, D. H. Edgell, J. E. Fair, M. Farrell, R. J. Fortner, J. Frenje, M. G. Gatu Johnson, E. Giraldez, V. Yu. Glebov, G. Grim, B. A. Hammel, A. V. Hamza, D. R. Harding, S. P. Hatchett, N. Hein, H. W. Herrmann, D. Hicks, D. E. Hinkel, M. Hoppe, W. W. Hsing, N. Izumi, B. Jacoby, O. S. Jones, D. Kalantar, R. Kauffman, J. L. Kline, J. P. Knauer, J. A. Koch, B. J. Koziowski, G. Kyrala, K. N. LaFortune, S. Le Pape, R. J. Leeper, R. Lerche, T. Ma, B. J. MacGowan, A. J. MacKinnon, A. Macphee, E. R. Mapoles, M. M. Marinak, M. Mauldin, P. W. McKenty, M. Meezan, P. A. Michel, J. Milovich, J. D. Moody, M. Moran, D. H. Munro, C. L. Olson, K. Opachich, A. E. Pak, T. Parham, H.-S. Park, J. E. Ralph, S. P. Regan, B. Remington, H. Rinderknecht, H. F. Robey, M. Rosen, S. Ross, J. D. Salmonson, J. Sater, D. H. Schneider, F. H. Séguin, S. M. Sepke, D. A. Shaughnessy, V. A. Smalyuk, B. K. Spears, C. Stoeckl, W. Stoeffl, L. Suter, C. A. Thomas, R. Tommasini, R. P. Town, S. V. Weber, P. J. Wegner, K. Widman, M.

- Wilke, D. C. Wilson, C. B. Yeamans, and A. Zylstra, *Phys. Plasmas* **20**, 070501 (2013).
- [37] M. S. Plesset and T. P. Mitchell, *Q. Appl. Math.* **13**, 419 (1956).
- [38] V. A. Smalyuk, T. Döppner, J. L. Kline, T. Ma, H.-S. Park, L. J. Atherton, L. R. Benedetti, R. Bionta, D. Bleuel, E. Bond, D. K. Bradley, J. Caggiano, D. A. Callahan, D. T. Casey, P. M. Celliers, C. J. Cerjan, D. Clark, E. L. Dewald, S. N. Dixit, D. H. Edgell, J. Frenje, M. Gatu-Johnson, V. Y. Glebov, S. Glenn, G. Grim, S. W. Haan, B. A. Hammel, E. Hartouni, R. Hatarik, S. Hatchett, D. G. Hicks, W. W. Hsing, N. Izumi, O. S. Jones, M. H. Key, S. F. Khan, J. D. Kilkenny, J. Knauer, G. A. Kyrala, O. L. Landen, S. Le Pape, B. J. MacGowan, A. J. Mackinnon, A. G. MacPhee, J. McNaney, N. B. Meezan, J. D. Moody, A. Moore, M. Moran, A. Pak, T. Parham, P. K. Patel, R. Petrasso, J. E. Ralph, S. P. Regan, B. A. Remington, H. F. Robey, J. S. Ross, B. K. Spears, P. T. Springer, L. J. Suter, R. Tommasini, R. P. Town, S. V. Weber, K. Widmann, J. D. Lindl, M. J. Edwards, S. H. Glenzer, and E. I. Moses, *Phys. Rev. Lett.* **111**, 215001 (2013).
- [39] S. P. Regan, R. Epstein, B. A. Hammel, L. J. Suter, H. A. Scott, M. A. Barrios, D. K. Bradley, D. A. Callahan, C. Cerjan, G. W. Collins, S. N. Dixit, T. Döppner, M. J. Edwards, D. R. Farley, K. B. Fournier, S. Glenn, S. H. Glenzer, I. E. Golovkin, S. W. Haan, A. Hamza, D. G. Hicks, N. Izumi, O. S. Jones, J. D. Kilkenny, J. L. Kline, G. A. Kyrala, O. L. Landen, T. Ma, J. J. MacFarlane, A. J. MacKinnon, R. C. Mancini, R. L. McCrory, N. B. Meezan, D. D. Meyerhofer, A. Nikroo, H.-S. Park, J. Ralph, B. A. Remington, T. C. Sangster, V. A. Smalyuk, P. T. Springer, and R. P. J. Town, *Phys. Rev. Lett.* **111**, 045001 (2013).

- [40] T. Ma, S. V. Weber, N. Izumi, P. T. Springer, P. K. Patel, M. H. Key, L. J. Atherton, L. R. Benedetti, D.K. Bradley, D. A. Callahan, P. M. Celliers, C. J. Cerjan, E. L. Dewald, S. N. Dixit, T. Döppner, D. H. Edgell, S. Glenn, G. Grim, S. W. Haan, B. A. Hammel, D. Hicks, W. W. Hsing, O. S. Jones, S.F. Khan, J. D. Kilkenny, J. L. Kline, G. A. Kyrala, O. L. Landen, S. Le Pape, B. J. MacGowan, A. J. Mackinnon, A. G. MacPhee, N. B. Meezan, J. D. Moody, A. Pak, T. Parham, H.-S. Park, J.E. Ralph, S. P. Regan, B. A. Remington, H. F. Robey, J. S. Ross, B. K. Spears, V. Smalyuk, L.J. Suter, R. Tommasini, R. P. Town, J. D. Lindl, M. J. Edwards, S. H. Glenzer, and E. I. Moses, *Phys. Rev. Lett.* **111**, 085004 (2013).
- [41] D. S. Clark, *et al.*, *Phys. Plasmas* **20**, 056318 (2013).
- [42] V. A. Smalyuk, D. T. Casey, D. S. Clark, M. J. Edwards, S. W. Haan, A. Hamza, D. E. Hoover, W. W. Hsing, O. Hurricane, J. D. Kilkenny, J. Kroll, O. L. Landen, A. Moore, A. Nikroo, A. Pak, J. L. Peterson, K. Raman, B. A. Remington, H. F. Robey, S. V. Weber, and K. Widmann, “First measurements of hydrodynamic instability growth in indirectly driven implosions at National Ignition Facility,” submitted to *Phys. Rev. Lett.*
- [43] V. A. Smalyuk, R. E. Tipton, J. E. Pino, D. T. Casey, G. P. Grim, B. A. Remington, D. P. Rowley, S. V. Weber, M. Barrios, R. Benedetti, D. L. Bleuel, D. K. Bradley, J. A. Caggiano, D. A. Callahan, C. J. Cerjan, D. H. Edgell, M. J. Edwards, J. A. Frenje, M. Gatu-Johnson, V. Y. Glebov, S. Glenn, S. W. Haan, A. Hamza, R. Hatarik, W. W. Hsing, N. Izumi, S. Khan, J. D. Kilkenny, J. Kline, J. Knauer, O. L. Landen, T. Ma, J. M. McNaney, M. Mintz, A. Moore, A. Nikroo,

- A. Pak, T. Parham, R. Petrasso, D. B. Sayre, M. Schneider, R. Tommasini, R. P. Town, K. Widmann, D. C. Wilson, and C. B. Yeaman, “Measurements of ablator-gas mix in indirectly driven implosions at National Ignition Facility,” submitted to *Phys. Rev. Lett.*
- [44] D. G. Hicks, *et al.*, *Phys. Plasmas* **19**, 122702 (2012).
- [45] H. F. Robey, *et al.*, *Phys. Plasmas* **19**, 042706 (2012).
- [46] S. H. Glenzer, *et al.*, *Phys. Plasmas* **19**, 056318 (2012).
- [47] S. Glenn, *et al.*, *Rev. Sc. Instrum.* **83**, 10E519 (2010).
- [48] D. B. Sayre, C. R. Brune, J. A. Caggiano, V.Y. Glebov, R. Hatarik, A. D. Bacher, D. L. Bleuel, D. T. Casey, C. J. Cerjan, M. J. Eckart, R. J. Fortner, J. A. Frenje, S. Friedrich, M. Gatu-Johnson, G. P. Grim, C. Hagmann, J. P. Knauer, J. L. Kline, D. P. McNabb, J. M. McNaney, J. M. Mintz, M. J. Moran, A. Nikroo, T. Phillips, J. E. Pino, B. A. Remington, D. P. Rowley, D. H. Schneider, V. A. Smalyuk, *Phys. Rev. Lett.* **111**, 052501 (2013).
- [49] R. M. Darlington, T. L. McAbee, and G. Rodrigue, *Comput. Phys. Commun.* **135**, 58 (2001).
- [50] G. Dimonte and R. Tipton, *Phys. Fluids* **18**, 085101 (2006).
- [51] R. H. H. Scott, *et al.*, *Phys. Rev. Lett.* **110**, 075001 (2013).
- [52] O O. L. Landen, R. Benedetti, D. Bleuel, T. R. Boehly, D. K. Bradley, J. A. Caggiano, D. A. Callahan, P. M. Celliers, C. J. Cerjan, D. Clark, G. W. Collins, E. L. Dewald, S. N. Dixit, T. Döppner, D. Edgell, J. Eggert, D. Farley, J. A. Frenje,

- V. Glebov, S. M. Glenn, S. H. Glenzer, S. W. Haan, A. Hamza, B. A. Hammel, C. A. Haynam, J. H. Hammer, R. F. Heeter, H. W. Herrmann, D. G. Hicks, D. E. Hinkel, N. Izumi, M. Gatu Johnson, O. S. Jones, D. H. Kalantar, R. L. Kauffman, J. D. Kilkenny, J. L. Kline, J. P. Knauer, J. A. Koch, G. A. Kyrala, K. LaFortune, T. Ma, A. J. Mackinnon, A. J. Macphee, E. Mapoles, J. L. Milovich, J. D. Moody, N. B. Meezan, P. Michel, A. S. Moore, D. H. Munro, A. Nikroo, R. E. Olson, K. Opachich, A. Pak, T. Parham, P. Patel, H.-S. Park, R. P. Petrasso, J. Ralph, S. P. Regan, B. A. Remington, H. G. Rinderknecht, H. F. Robey, M. D. Rosen, J. S. Ross, J. D. Salmonson, T. C. Sangster, M. B. Schneider, V. Smalyuk, B. K. Spears, P. T. Springer, L. J. Suter, C. A. Thomas, R. P. J. Town, S. V. Weber, P. J. Wegner, D. C. Wilson, K. Widmann, C. Yeamans, A. Zylstra, M. J. Edwards, J. D. Lindl, L. J. Atherton, W. W. Hsing, B. J. MacGowan, B. M. Van Wonterghem, and E. I. Moses, *Plasma Phys. Controlled Fusion* 54, 124026 (2012).
- [53] S. W. Haan, *et al.*, *Fus. Sci. and Tech.* 63, 67 (2013).
- [54] S. V. Weber, *et al.*, “NIF symmetry capsule modeling”, *Bull. Am. Phys. Soc.* **58**, 195 (2013).
- [55] D. S. Clark, *et al.*, “Progress in modeling ignition experiments on the National Ignition Facility”, to be published in the Proceedings of the Eighth International Conference on Fusion Sciences and Applications, Nara, Japan (2013).

FIGURE CAPTIONS

FIG. 1 (Color online). Experimental configuration schematically shows the target including Au hohlraum, plastic (CH) capsule, Au cone, and the vanadium backlighter. The gold cone provided a possibility for the backlighter x-rays to pass through a single wall of the shell.

FIG. 2 (Color online). A picture of the capsule with pre-imposed 2D modulations and a gold cone oriented along a diagnostic line of sight. The outer circular feature is the equatorial diagnostic band before hohlraum assembly.

FIG. 3. The laser pulse shape used in the experiments for hohlraum drive had a peak power of ~ 350 TW and total energy of ~ 1.3 MJ.

FIG. 4 (Color online). Measured capsule x-ray radiographs captured on a framing camera. The central four images were formed using 20- μm wide slit, while images on right and left sides of the slit images were formed with 20- μm and 50- μm pinholes. This experiment was performed with side-by-side mode 60 (initial wavelength of 120 μm) and mode 90 (initial wavelength of 80 μm) modulations.

FIG. 5 (Color online). Evolution of the measured (symbols) and simulated (solid curves) amplitudes of the optical-depth modulations as a function of measured modulation wavelength for (a) mode 30 with initial wavelength of 240 μm and amplitude of 0.75 μm , (b) mode 60 with initial wavelength of 120 μm and amplitudes of 1.7 and 0.25 μm , and (c) mode 90 with initial wavelength of 80 μm and amplitude of 0.3 μm .

FIG. 6 (Color online). Measured (symbols) and calculated (solid curve) linear growth factors for optical-depth modulations as a function of the modulation mode number are shown at a shell radius of 650 μm , corresponding to a measurement time of 20.3 ns.

FIG. 7 (Color online). Capsule schematics (a) with 4- μm thick CD layer and (b) without CD layer (“CH capsules”). The CD layer was placed either at the inner shell surface, or recessed from the inner surface by 1.2, 2.3, 3.9, and 8.0 μm of CH layers. The capsules were filled with tritium gas with mass density of 11.05 mg/cc at temperature of 32K.

FIG. 8 (Color online). Laser pulse shape used in the experiments with peak power of ~ 436 TW and total energy of ~ 1.5 MJ.

FIG. 9 (Color online). Measured neutron spectrum for implosion with the 4- μm CD layer showing DT neutron peak at ~ 14 MeV, down-scattered neutron region between 10 and 12 MeV, and TT neutron region below 9 MeV.

FIG. 10 (Color online). Measured and simulated (a) DT neutron yield, (b) the ion temperature inferred from the time-of-flight broadening of the DT fusion yields, and (c) TT neutron yield, as a function of recession depth of the CD layer, and for CH capsules without a CD layer. Also shown are results of 2D ARES simulations including a K-L mix model, with three initial turbulent mixing length of $L_0=0.1$ nm (solid curve). The blue squares represent simulations of the CH capsules. The measurements are shown by the solid symbols.

Figure 1

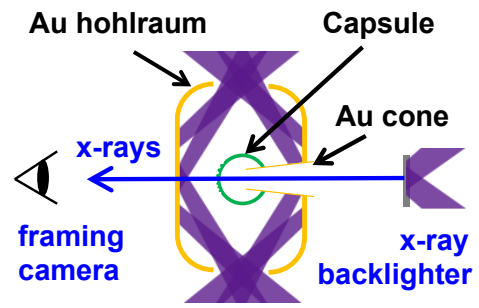


Figure 2

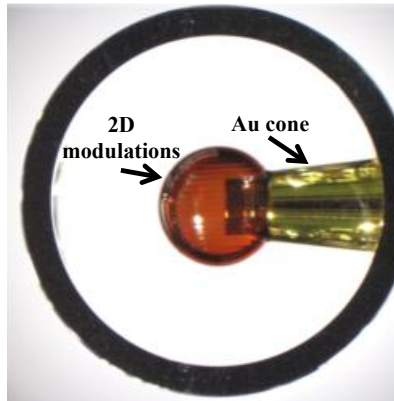


Figure 3

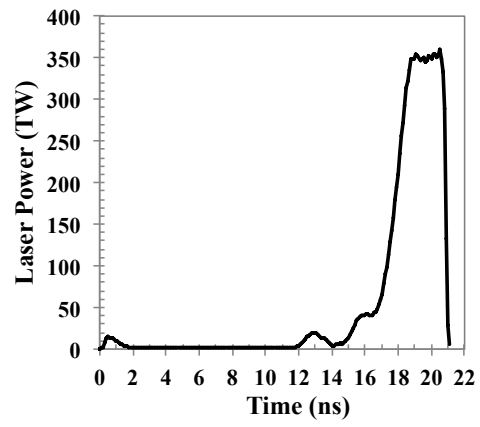


Figure 4

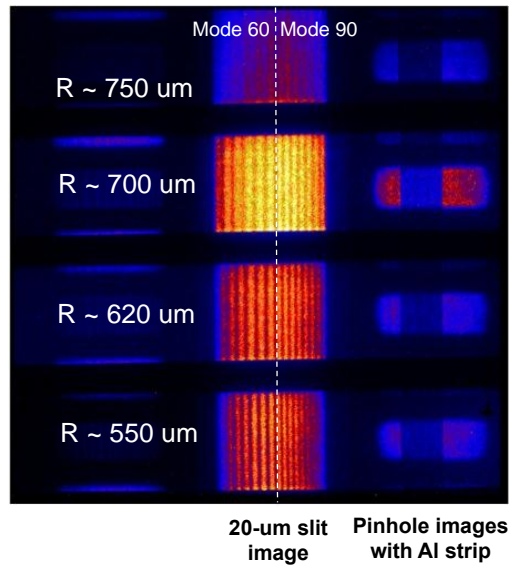


Figure 5

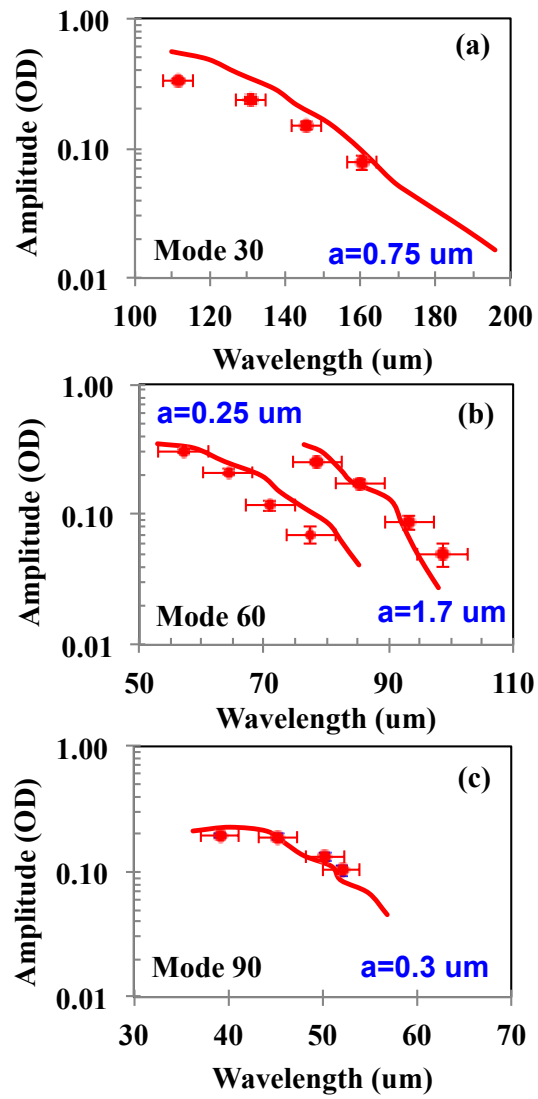


Figure 6

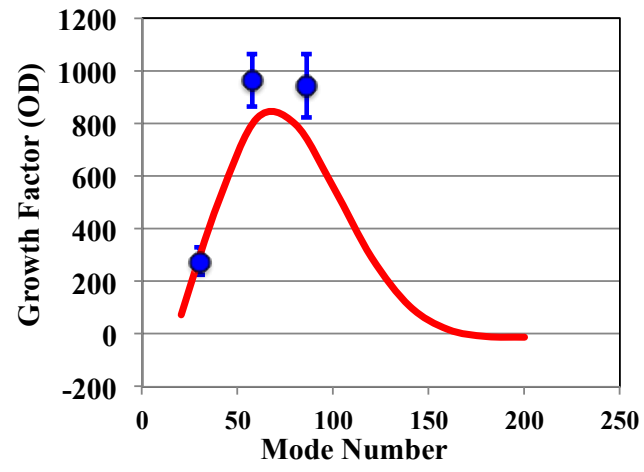


Figure 7

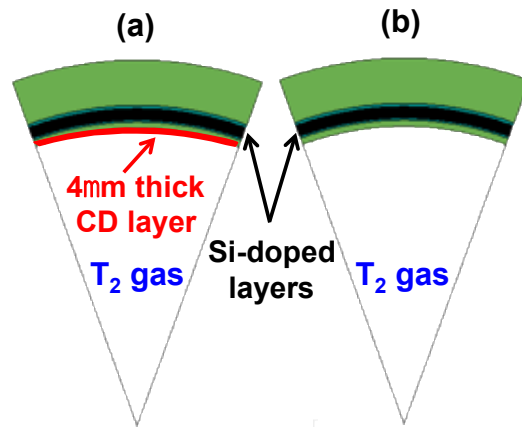


Figure 8

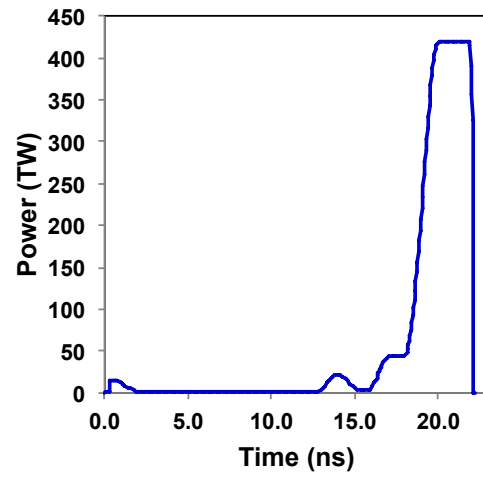


Figure 9

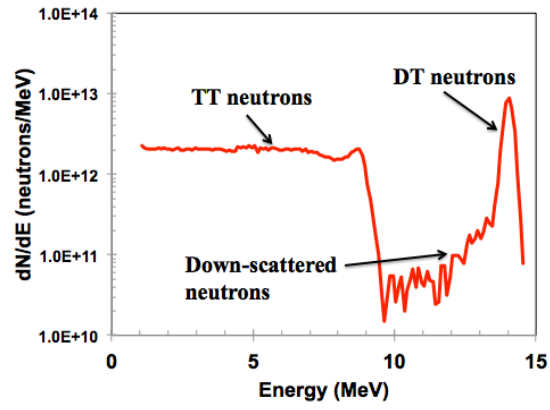


Figure 10

